Research Article

Can we correct optical light measurements only using radio-based relations?

EMU/GAMA: Refining dust extinction corrections for Hα luminosity functions using radio-based star formation rates

That's me!

Jayde Willingham[1,2], Andrew Hopkins[1,2], Tayyaba Zafar[1,2,3], José Afonso[4,5], Ummee Tania Ahmed[2,6,7], Adeel Ahmad[8], Andrew Battisti[9,10,3], Dominik J. Bomans[11,12], Michael Brown[13], Michael Cowley[7,14], Duncan Farrah[15,16], Tim Gúthe[11,12], Jeremy Mullaney[17], Bärbel S. Holwerda[19], Denis Leahy[20], Umberto Maio[21,22], Tamal Mukherjee[1,2,3], Jahang Prathap[1,2,3], Nicholas Seymour[17], Jacco Th. van Loon[23] and Ethan Ward[1,2]

[1]School of Mathematical and Physical Sciences, Macquarie University, Australia, [2]Astrophysics and Space Technologies Research Centre, Macquarie University, Australia, [3]ARC Centre of Excellence for All Sky Astrophysics in 3 Dimensions (ASTRO-3D), Australia, [4]Instituto de Astrofisica e Ciências do Espaco, Universidade de Lisboa, Portugal, [5]Departamento de Física, Faculdade de Ciências, Universidade de Lisboa, Portugal, [6]Australian Astronomical Optics, Macquarie University, Australia, [7]Centre for Astrophysics, University of Southern Queensland, Australia, [8]School of Science, Western Sydney University, Australia, [9]Research School of Astronomy and Astrophysics, Australian National University, Australia, [10]International Centre for Radio Astronomy Research (ICRAR), The University of Western Australia, Australia, [11]Ruhr Astroparticle and Plasma Physics Center (RAPP Center), Germany, [12]Fakultät für Physik und Astronomie, Astronomisches Institut (AIRUB), Ruhr-Universität Bochum, Germany, [13]School of Physics, Monash University, Australia, [14]School of Chemistry and Physics, Faculty of Science, Queensland University of Technology, Australia, [15]Department of Physics and Astronomy, University of Hawai'i at Mānoa, USA, [16]Institute for Astronomy, University of Hawai'i at Manoa, USA, [17]International Centre for Radio Astronomy Research, Curtin University, Australia, [18]CSIRO Space and Astronomy, Australia, [19]Leiden Observatory, Leiden University, Netherlands, [20]Physics and Astronomy, University of Calgary, Canada, [21]INAF – Observatory of Trieste, Italy, [22]IFPU – Institute for Fundamental Physics of the Universe, Italy and [23]Lennard-Jones Laboratories, Keele University, UK

A lot of people helped to shape this paper, from all different parts of the global research community!

The key idea:

We measure the relationship between uncorrected, optically derived star formation rates and intrinsically dust-corrected radio-derived star formation rates and use this empirical relation to infer corrections for galaxies out to high redshift. The resulting star formation rate densities are systematically overpredicted at high redshift, implying that the dust properties of local and high-redshift galaxies must differ fundamentally.

Background Information:

Galaxies tell us a lot about the universe!

Star formation within galaxies is a very important property and process.

Therefore, we NEED new and accurate ways to correct measurements of it - especially when our data is from galaxies super far away!

Corresponding author: Jayde Willingham; Email: jaydewillingham1@gmail.com.

Cite this article: Willingham J, Hopkins A, Zafar T, Afonso J, Ahmed UT, Ahmad A, Battisti A, Bomans DJ, Brown M, Cowley M, Farrah D, Galvin T, Holwerda BW, Leahy D, Maio U, Mukherjee T, Prathap J, Seymour N, Van Loon JT and Ward E. (2026) EMU/GAMA: Refining dust extinction corrections for Hα luminosity functions using radio-based star formation rates. *Publications of the Astronomical Society of Australia*, 1. https://doi.org/10.1017/pasa.2026.10183

This page outlines the key concepts involved in correcting the observed light from distant galaxies and converting it into a physically meaningful measure of the star formation rate.

dust (Kennicutt 1998). The most commonly used approaches for estimating SFR consider UV, Hα, IR, and radio wavelength calibrations, while the single most ideal, extensively researched and widely applied SFR tracer is the Hα emission line (e.g. Kennicutt et al. 2001; Bell 2003; Hopkins 2004; Calzetti et al. 2007; Kennicutt et al. 2009; Boquien et al. 2016; Davies et al. 2016; Davies et al. 2017; Brown et al. 2017).

A powerful and widely used SFR tracer in the optical regime is the Hα emission line. This line arises from recombination in H II regions that are ionised by UV photons from high-mass, short-lived O and B stars ionise surrounding hydrogen gas. Because massive stars have lifespans of $\lesssim 10$ Myr, Hα emission line directly traces recent and ongoing star formation (Glazebrook et al. 1999; Kennicutt & Evans 2012). Hα emission is relatively insensitive to dust attenuation, which necessitates corrections. Accurate measurement of Hα flux also requires accounting for underlying stellar absorption, where the absorption features from older stellar populations partially fill in the emission line. Correcting for dust attenuation effects depends on the quality of the stellar continuum modelling and subtraction, which can be challenging, particularly in large spectroscopic surveys.

One of the most widely used tools to infer dust attenuation is the Balmer decrement (Hα/Hβ), which provides a basis for correcting dust-affected emission line fluxes. Balmer decrement corrections are typically applied to star-forming galaxies dominated by massive stars (Osterbrock 1989). The BD method relies on comparing the observed Balmer emission line ratio (typically Hα/Hβ) to the theoretically predicted case B recombination value, with any excess reddening interpreted as dust attenuation. By adopting an extinction law, the wavelength-dependent obscuration can then be quantified and applied to correct emission-line derived SFRs.

A limitation of the BD method is that it typically assumes a uniform dust screen geometry and treats the galaxy as optically thin. Many galaxies exhibit complex, clumpy dust distributions and optically thick central regions, which may lead to underestimated dust corrections (e.g. Calzetti et al. 2001; Reddy et al. 2013; Robertson et al. 2024). Reliable measurements require high signal-to-noise detections of both Hα and Hβ emission lines, which can be challenging, especially for high-redshift or faint galaxies. Furthermore, the choice of emission lines can also introduce significant biases in line ratio diagnostics (Yuan, Kewley, & Rich 2013). At higher redshifts, detections of both Hα and Hβ remain uncommon, with surveys such as HETDEX reporting only three confirmed LAEs at $z \gtrsim 2$ (of which only two have multiple rest-frame optical emission lines detected) (Finkelstein et al. 2011). Despite these challenges, Balmer decrement corrections are particularly valuable for star formation studies due to their ability to penetrate the dust that often obscures the most intense star-forming regions. Dust emission is not a direct tracer of star formation activity, its utility as a SFR indicator is strongly established by its correlation with radio and far infrared (FIR) luminosities in star-forming galaxies (Condon 1992; Yun, Reddy, & Condon 2001; Bell 2003; Jarrett et al. 2010; Molnar et al. 2021). In addition, radio emission has also been shown to correlate well with dust-corrected Hα luminosities (e.g. Murphy et al. 2011), further reinforcing its connection to recent massive star formation and providing a useful bridge between radio and traditional recombination line tracers. Previous studies have also directly calibrated Hα against FIR emission at z ∼ 0, providing important benchmarks for dust-corrected SFR estimates (e.g. Sobral et al. 2013; Ibar et al. 2013). These comparisons highlight both the potential and limitations of using FIR as a reference, motivating the need for refined dust corrections when relying on Hα at higher redshift.

Radio emission has traditionally been studied at 1.4 GHz, though with the advent of the Square Kilometre Array pathfinder telescopes and programmes, this is rapidly expanding to higher frequencies. Radio emission at frequencies lower than a few GHz is dominated by non-thermal synchrotron radiation produced by cosmic-ray electrons accelerated in supernova remnants. This is an indirect tracer of recent massive star formation over timescales of ∼40–100 Myr (Murphy et al. 2011). At higher frequencies, the thermal free-free emission contributes an increasing fraction of the total radio continuum. This emission originates from ionised gas in H II regions and directly traces massive star formation, analogous to Hα or Hβ. Around ∼ 30 GHz, the free-free and synchrotron components become comparable in strength (Condon 1992).

Contamination from AGN can complicate interpretations, necessitating careful source classification (Cowley et al. 2016). Once dust extinction is accounted for, Hα has relatively few assumptions for the conversion to SFR (i.e. recent star formation history and initial mass function) and thus is less susceptible to systematic errors than some tracers. The relative insensitivity of radio emission to dust obscuration raises the possibility that statistical measurements of star formation in the radio could be used to inform dust obscuration corrections for optical tracers like Hα, but this approach has not been comprehensively explored.

Despite its strengths as a robust and relatively straightforward dust obscuration correction in measurements of star formation, particularly at $z < 2.5$, Hα and Balmer decrement methods become increasingly challenging (Sanders et al. 2024). Dust correction is likely the single dominant source of uncertainty at intermediate redshifts $1 < z < 5$, which means an empirical SFR based dust correction method, that is dependent on luminosity and redshift, could have significant impact in this epoch. This need is motivated by the frequent absence of wavelength coverage and/or sufficient signal-to-noise to perform Balmer decrement–based corrections for individual galaxies in current deep surveys (e.g. Reddy et al. 2023; Matharu et al. 2023; Shapley et al. 2023). To address this limitation, empirical calibrations between Hα luminosity and radio tracers in the local Universe (e.g. Hopkins et al. 2001, Ahmed et al. in prep) can be applied to extend dust-correction techniques to the early Universe, where the *James Webb Space Telescope* (*JWST*) and *Roman* are expected to have the ability to probe star-forming galaxies, enabling detailed observations of dust-obscured star formation (e.g. Wang et al. 2019). Such surveys offer a vital dataset for studying the evolution of star formation through Hα emission at the earliest epochs provided that robust obscuration corrections can be established. To this end, we adopt a model for luminosity dependent obscuration anchored in the local region and progressively reduce its strength with redshift, using the cosmic star formation history as a constraint. This approach allows us to test whether a single, physically motivated luminosity dependent obscuration in Hα, thereby enabling physically motivated corrections applicable to large galaxy samples.

The layout of this paper is as follows. In Section 2 the radio and optical data used in order to fit a SFR tracer relationship is introduced. In this same section a compilation of published Hα luminosity function results are presented, along with details

People use all different wavelengths to measure star formation!

A good option is Hα as it emitted from young, short-lived stars. The strength can help us infer how many stars were recently born.

HOWEVER optical light is affected by dust surrounding the galaxies it originated from. Dust absorbs starlight and reemits it at higher wavelengths.

One goal of this paper is to find a different way to change the light back.

Some people use the Balmer Decrement to correct for dust which is a theoretical ratio of emission lines that can help us see how much our light is affected by dust. At high redshift, this option is often not feasible!

Okay, so we could use radio wavelengths instead – radio passes through dust without being affected and has been shown to correlate well with infrared and optical baby starlight!

This method can't be perfect. We may get affected by AGN and other processes that give off radio wavelengths.

But is there a way we can use this correlation to correct the optical data we already have?! (... This is what this paper is about). Can we also see if this correlation changes based on the strength of the baby starlight and if it changes based on how long ago the light was emitted (... also yes!)

Star Formation Rate = SFR

on dust correction removal and IMF conversion where needed. [illegible] Hα luminosities is introduced and applied to published work. The [illegible] function (LF) and star formation rate density (SFRD) evolution [illegible]. Throughout this paper, cosmological parameters of $H_0 = 70$ km s^{-1} Mpc^{-1}, $\Omega_M = 0.3$, $\Omega_\Lambda = 0.7$, and $\Omega_k = 0$, a convenient approximation to recent measurements (e.g. Planck Collaboration et al. 2016). Adopting more precise cosmological values does not change any of our analysis measurably. We adopt a Chabrier IMF, converting other published results to this IMF as needed.

Here we say that we assume a common stellar initial mass function – this removes a source of bias!

What data did we use?

This analysis requires data from multiple catalogues to create a multiwavelength study of star forming galaxies (SFGs) that connects the obscured Hα SFR tracer to the unobscured radio SFR tracer, for the same set of sources over a large enough coverage for a statistical study. We use early science radio data from the Evolutionary Map of the Universe (EMU; Norris et al. 2021; Hopkins et al. 2025), focusing on the G23 field. This dataset is integrated [illegible] SFR data from the Galaxy and Mass Assembly (GAMA) survey (Driver et al. 2009, 2011, [illegible]) [illegible] in a redshift range of $0.0 < z < 0.35$,[a] is used to compare uncorrected Hα-based SFRs to radio-derived (1.4 GHz) SFRs, which serve as a dust-unbiased reference. Given that the radio luminosity is unaffected by dust obscuration we adopt it as a proxy for the corrected SFR measure for Hα. This analysis is then used to correct, or recorrect, for dust obscuration in other published Hα luminosity function studies spanning the last ∼30 yr.

Step 1: Make the uncorrected optical vs naturally corrected radio relationship!

Evolutionary Map of the Universe:

The EMU is an ongoing radio continuum survey (Hopkins et al. 2025) [illegible] providing a comprehensive view of the Southern sky using the Australian Square Kilometre Array Pathfinder (ASKAP) telescope (Johnston et al. 2007; McConnell et al. 2020). [illegible] employs an array of 36 × 12 m antennas, covering baselines from 22 to 6 000 m. This configuration enables observations [illegible] 80 MHz frequency range and an instantaneous bandwidth of 288 MHz. EMU's use of ASKAP is expected to catalogue [illegible] 0 sources, creating the most comprehensive atlas of the southern sky, with an angular resolution of [illegible] FWHM and a sensitivity of roughly 20 μJy beam^{-1}.

EMU is the radio data survey we use for the naturally corrected measurement part.

For this study, we use EMU early science observations from the GAMA G23 field, (Gürkan et al. 2022); see also Heaney et al. (2019) for earlier technical details. The G23 region centred at $\alpha = 23$ h and $\delta = -32°$, spans an area of 82.7 deg^2 with observations at a frequency of 887.5 MHz and a sensitivity of 0.038 μJy beam^{-1}. The G23 radio data are matched with the GAMA catalogue to support our analysis.

Galaxy and Mass Assembly:

The GAMA survey comprises photometric and spectroscopic data across five sky fields (G02, G09, G12, G15, and G23), covering a total area of approximately 280 deg^2. Spectroscopic data were obtained using the AAOmega spectrograph on the Anglo-Australian Telescope (AAT), which supports a maximum of 400 fibres and spectral resolution of up to 10 000 (Smith et al. 2004; Sharp et al. 2006). Of particular interest for this study is the G23 field that covers 82.7 deg^2 ($339° < RA < 351°$, $-35° < \delta < -30°$), with a limiting magnitude of $i < 19.2$ mag at a frequency of 887.5 MHz and was targeted for early science observations from EMU [illegible].

GAMA is the optical survey where we get all the Hα data!

We use the latest data from the GAMA Data Release 4 (DR4) in this analysis, accessing three primary catalogues stored in data management units (DMUs) (Bellstedt et al. 2020; Driver et al. 2022). [illegible] Sersic Catalogue v23 (Kelvin et al. 2012), which includes data on stellar masses, rest-frame photometry, and pop- [illegible] synthesis fits [illegible] five surveys [illegible] (Taylor et al. 2011). Photometric data for the G23 field are obtained from the [illegible] DMU, which integrates data from the European Southern Observatory's (ESO) Visible and Infrared Survey Telescope for Astronomy (VISTA) Kilo-Degree Infrared Galaxy Public Survey (VIKING; Edge et al. 2013) and the ESO VST Kilo Degree Survey (KiDS; Jong et al. 2013). GKV (GAMA-KiDS-VIKING), provides multiwavelength photometry spanning from the FUV, using the Galaxy Evolution Explorer (GALEX) space telescope (100–200 nm; Liske et al. 2015), to the second WISE band (W2; 4.6 μm; Wright et al. 2010). This DMU is not directly accessed here but is integral to related and ongoing studies of this dataset, including applications such as spectral energy distribution fitting. Emission line fluxes and equivalent width measurements are accessed from the `GaussFitSimplev05` DMU (Gordon et al. 2017). This catalogue employs multiple Gaussian fits to enhance accuracy. Previous studies have shown that simpler models yield comparable quantitative results (Ahmed et al. 2024).

The important part is that both data sets are from the local universe. (Keep this in mind)

Selecting the good data:

This study focuses on comparing SFR estimators that draw on a diverse set of parameters. To achieve this, GAMA data was cross-matched with that from EMU within the G23 field. In order to achieve this multiwavelength approach, several GAMA catalogues [illegible] spectral or catalogue IDs, leading to a total of 25 762 GAMA sources with emission line and photometric data. A 5″ [illegible] cross-match with the EMU catalogue, motivated by the cross-match success curves from Ahmed et al. (2024), yielded a 'parent sample' of [illegible] sources.

Here we outline all the quality assurance checks we do to make sure our data is good enough to make bold statements! We also cite places that have shown statistically why these are good and important to do.

The parent sample was refined using several quality assurance [illegible] resulting in a final sample of [illegible] sources. A detailed explanation of the criteria used is presented here.

[illegible] Balmer lines, Hα and Hβ, as well as the NII and OIII emission lines [illegible] BPT diagram (Baldwin et al. 1981). [illegible] ation threshold was established to ensure accurate calculations of luminosities [illegible] SFRs. Additionally, the emission line fluxes were required to meet a signal-to-noise (S/N) ratio threshold of $S/N > 3$. These cuts are the deepest impact to the sample size but it should guarantee that this work is built on a quality dataset.

Redshift is necessary for calculating luminosities. Redshift quality is assessed using the parameter $nQ \geq 3$ which corresponds to a redshift of at least 90% confidence (Liske et al. 2015). After applying this criterion, relevant equivalent widths were tested for positivity, and a ceiling was applied to the emission line fluxes.

[a]The redshift range is limited by the ability to detect the Hα line in the wavelength range of the AAOmega spectrograph on the AAT (Driver et al. 2011).

BPT Diagram: This is a tool to check that our sources' light is from stars and not some other process.

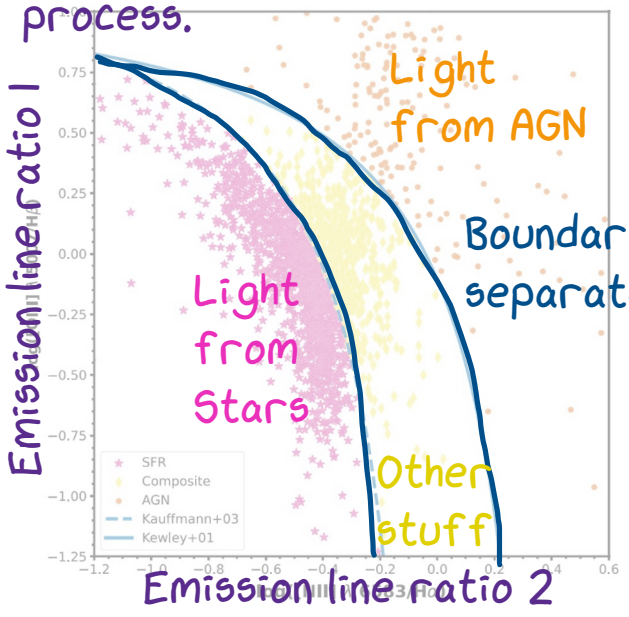

Figure 1. The BPT diagram, which uses the [OIII]/Hβ and [NII]/Hα emission line ratios, classifies galaxies as star-forming galaxies (SFGs), active galactic nuclei (AGNs), or composite sources. SFGs, represented by pink stars, lie below the dashed blue Kauffmann line; AGNs, represented by orange circles, are positioned above the solid blue Kewley line; and composite sources, shown as yellow diamonds, are located between the two diagnostic lines. These sources are drawn from the EMU and GAMA catalogues and were processed as described in Section 2.

We use a few diagnostic tools based on emission line ratios, so one check we do is to make sure we are looking at sources with emission line and not absorption lines!

We also make sure we have good signal to noise, that the redshift measurements are of high quality, and that there are no NaN or saturated values that have crept in from the telescopes.

3. Redshift quality is checked for nQ ≥ 3. (1 736 sources)
4. Positive detection of the Hα and Hβ equivalent widths (EW). (1 734 sources)
5. Ceiling values for Hα and Hβ Balmer lines are removed. (1 726 sources)
6. 'IS_BEST' flag is true. (1 687 sources)
7. SFGs are classified and extracted using the BPT diagram (AGNs and composite galaxies are removed from the sample). (1 036 sources)

This results in a sample of 1 036 SFGs with radio detections in G23.

Luminosity Densities

We compiled published Hα luminosities from a broad range of studies (Tresse & Maddox 1998; Shioya et al. 2008; Sullivan et al. 2000; Morioka et al. 2008; Fujita et al. 2003; Stroe & Sobral 2015; Pa[illegible] et al. 2005; Lee et al. 2007; Gallego et al. 1995; Sobral et al. 2013; Hippelein et al. 2003; Drake et al. 2013; Gómez-Guijarro et al. 2016; Yan et al. 1999; Hopkins, Connolly, & Szalay 2000; Villar et al. 2008; Ly et al. 2007; Hayes, Schaerer, & Östlin 2010; Lee et al. 2009; Sun et al. 2023; Bollo et al. 2023; Covelo-Paz et al. 2025; Koyama et al. 2013; Shim et al. 2011) that span a wide range of research and covering a wide range of redshifts ($z = 0 - 8$). The inclusion of high-redshift data allows for a test of our novel dust correction method for Hα LFs at the highest observed redshifts.

Where possible, we used observed Hα LFs uncorrected for dust obtained from published tabulated LF values, luminosity density values directly. For datasets published only as figures, we digitised the luminosity functions and extracted luminosity density values manually. In cases where only dust-corrected values were available, we reversed the applied corrections detailed in the published work. The most commonly used correction was the scaling factor from Calzetti et al. (2000), which we removed to approximate the uncorrected luminosity. In some cases only the average Calzetti correction value was reported, for which we had to assume this in the de-correction across all samples. If insufficient information was available to de-correct dust corrections, the published data was excluded in this work. We also noted the IMF assumption used in each study. For any work that included a SFRD calculation adopting the Salpeter (1955) IMF, we applied the conversion factor (0.63) to bring all estimates to a common Chabrier (2003) IMF following the methodology outlined in Madau & Dickinson (2014). It is also worth noting that all published luminosity functions were fitted with single Schechter functions, and all fit parameters were homogenised to consistent units.

Once we make our relationship, we want to apply it to Hα luminosity densities. These luminosity densities are used to calculate the star formation rate density over cosmic time, which is our real end goal!

Note: Luminosity ∝ SFR

Correcting for Dust

The aim of this work is to use the relationship between obscured (Hα) and unobscured (radio) SFRs in order to find a self consistent method for dust correction where spectroscopy or colour correction methods are not applicable. This need comes from the increasing numbers of large rest-frame UV-optical surveys, where dust corrections are difficult to make. Such is the case for the [illegible] which are redshifted beyond the observable wavelength range or have poor S/N (e.g. Reddy [illegible] Shivaei et al. 2015; Shapley et al. 2022). This section details the process we follow to establish a relationship in the SFR

Our relationship works by taking an uncorrected Hα SFR and finding its corresponding naturally corrected radio SFR. We can then switch between Luminosity and SFR simply!

between Hα and 1.4 GHz radio wavelength tracers. This relationship enables us to convert uncorrected SFRs into dust-corrected values and thereby recover the corresponding inferred intrinsic Hα luminosities. In addition, we explore three alternative models in which the slope of the relationship is varied, providing a means to test its use as a proxy for dust content.

While both Hα and radio continuum emission are widely used to trace star formation, they probe different physical processes and timescales. Hα emission traces ionising photons from massive stars with lifespans $\lesssim$10 Myr, providing a snapshot of very recent star formation. In contrast, radio emission at 1.4 GHz is primarily non-thermal synchrotron radiation from supernova remnants, traces star formation over longer timescales (∼10–100 Myr; Kennicutt & Evans 2012). The timescale offset can contribute to discrepancies in galaxies with bursty or rapidly changing star formation histories, where the current star formation activity is poorly traced by delayed radio emission. For example, in recently quenched systems, radio emission can persist for ∼100 Myr leading to overestimate of the present-day SFR compared to Hα (Arango-Toro et al. 2025).

In galaxies with relatively continuous star formation over these timescales, typical of many star-forming galaxies in the local universe, the tracers are found to correlate well. Duncan et al. (2020) found the relationship between Hα and radio luminosity shows no significant evolution out to redshift $z \sim 2.6$, providing empirical calibration for the majority of a substantial fraction of cosmic history. Cook et al. (2024) demonstrate that calibrating [illegible] requires careful consideration of the timescale sensitivity of each tracer, especially when comparing to IR or UV-based measurements. The [illegible] differences across galaxy populations and redshifts remains an open question, and continued observational and theoretical work will be key to understanding where and when these tracers may diverge. The choice of SFR calibration introduces an additional source of uncertainty, as [illegible] can significantly impact both SFR and SFRD estimates, particularly at higher luminosities (e.g. Matthews et al. 2021). In this work we adopt the calibrations of Kennicutt (1998) and Bell (2003), though alternative empirical relations could also be explored. With sufficiently broad photometric coverage, spectral energy distribution fitting provides another avenue for deriving consistent SFR estimates.

Despite these limitations, a SFR-dependent obscuration correction offers promising potential as a flexible and observationally grounded tool for estimating SFRs, especially in regimes where traditional dust corrections are inaccessible or unreliable. Unlike fixed attenuation laws or colour-based [illegible], this method directly links two widely observable quantities: observed Hα luminosity, which is sensitive primarily to the unobscured component of recent star formation (and requires extinction correction to recover the total), and 1.4 GHz radio luminosity, which is largely insensitive to dust and therefore traces the total star formation (both obscured and unobscured). When calibrated properly, this approach could bridge datasets from UV/optical and radio surveys in a self-consistent way and be deployed in large-scale survey pipelines where full SED fitting is not feasible.

Calculating Star Formation Rates using Radio Wavelengths

To compare against optical-continuum-based SFRs, we require flux density at 1.4 GHz. Since the early science EMU catalogue provides data at 888 MHz, we convert to 1.4 GHz assuming a spectral index[b] of $\alpha = -0.7$. Varying this assumption has a negligible effect on the final result. Once these conversions are made, the radio luminosity can be calculated using

$$L_{1.4\,\mathrm{GHz}} = \frac{4\pi D_L^2 S_{1.4}}{(1+z)^{1+\alpha}}, \quad (1)$$

where D_L [pc] is the luminosity distance, $S_{1.4}$ [W Hz^{-1}] is the radio flux, and z is the redshift.

The conversion is then applied using the relation derived by Bell (2003), which is based on the correlation between radio and [illegible] (Kennicutt et al. 2003),

$$\mathrm{SFR}_{1.4\,\mathrm{GHz}}[\mathrm{M}_\odot\,\mathrm{yr}^{-1}] = \begin{cases} \dfrac{L_{1.4\,\mathrm{GHz}}\,[\mathrm{W\,Hz^{-1}}]}{1.81\times10^{21}} & \text{for } L > L_c, \\ \dfrac{L_{1.4\,\mathrm{GHz}}\,[\mathrm{W\,Hz^{-1}}]}{[0.1+0.9(L/L_c)^{0.3}]\cdot 1.81\times10^{21}} & \text{for } L \le L_c, \end{cases} \quad (2)$$

where $L_c = 10^{21.53}$ W Hz^{-1}. Bell uses a step-function-based correction based on a galaxy's 1.4 GHz luminosity. The luminosity traces both thermal synchrotron emission from [illegible] remnants, which correlates with recent star formation. The correlation is strong in star-forming galaxies but less reliable in quiescent galaxies, where the emission may originate from old stars or AGN. The step function in Equation (2) helps avoid overestimating the SFR in such cases. This [illegible] Bell (2003) method remains broadly consistent other radio-SFR based calibrations within 20–30%, depending on assumptions such as IMF, radio frequency, and treatment of thermal emission (e.g. Murphy et al. 2011; Delhaize et al. 2017). As radio wavelengths are unobscured by dust, this SFR acts as the naturally dust corrected SFR.

Calculating Star Formation Rates using Optical Wavelengths

The SFRs from Hα emission are derived in order to compare with their radio counterparts. Equations (3) and (4) are first applied to correct for several observational systematics. The Hα luminosity is then calculated following the methods outlined in Hopkins et al. (2003) and Gunawardhana et al. (2011). Including correcting for stellar absorption and for the aperture losses associated with fibre spectroscopy. We do not apply a dust extinction correction here in order to replicate conditions where such steps are unavailable, thus Balmer Decrement corrections are omitted (Gunawardhana et al. 2011).

$$A_{H\alpha} = (2.35 \times 10^{-10}) \times \frac{3\times10^{11}}{[6563.61(1+z)]^2} \quad (3)$$

The common equivalent width correction (AW_λ) is assumed to be 1.3 Å, (Gunawardhana et al. 2013). The absolute magnitude in the r-band (M_r) is provided by the GAMA survey.

The Hα luminosity is then used to estimate uncorrected SFR as derived by Kennicutt (1998):

$$\mathrm{SFR}_{H\alpha}[\mathrm{M}_\odot\,\mathrm{yr}^{-1}] = \frac{L_{H\alpha}\,[\mathrm{W\,Hz^{-1}}]}{7.9\times10^{35}}. \quad (4)$$

[b]We adopt the convention $S \propto \nu^{\alpha}$.

This whole section basically justifies why we can use this simple relationship to do a pretty complex correction. We discuss the different physical processes the two types of light trace and how they trace processes that occur on different timescales. Despite all that we show studies where they still correlate, but it is still something to consider.

Here we show how we take our raw EMU radio data and turn it into a SFR to construct this relationship we keep talking about.

Essentially: Flux -> Luminosity -> SFR

Through different scaling relations!

This details how we take GAMA optical light to SFR, which is basically the same process but there are a few more signal corrections to do.

Uncorrected optical vs naturally corrected radio SFR relationship

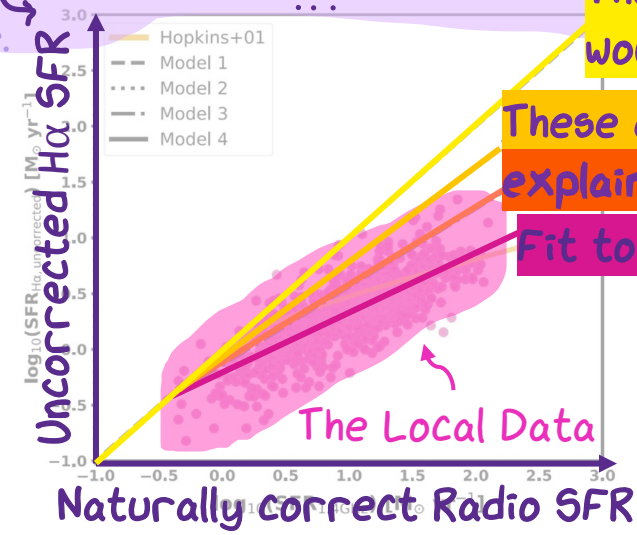

The line where SFRs are equal which would only happen if there is no dust!

These are two lines that might explain high redshift data.

Fit to the local data

Figure 2. The relationship between Hα and 1.4 GHz radio tracers of star formation. Four models are shown: the solid line is the best-fit relation to the local EMU-GAMA SFG sample, while the dashed line marks the 1:1 case, where Hα and radio SFRs would be equal, making the 1:1 line the dust free line. The dotted and dot-dashed lines represent proposed interim models. For each model, the redshift interval over which its dust-corrected results align with the published SFRD measurements from Figure 4 is indicated. The truncated equation for each model is shown here for reference but can be seen in full in Table 1. The calibration from Hopkins et al. (2001) is shown in orange.

How are these Star Formation Rates related? -

We plot the two different star formation rates and then fit a simple linear relation to the data.

As you can see there is a strong correlation!

This line is basically a way to describe how much dust there is in the universe by how far it deviates from the one-to-one line.

$$\log_{10}(\mathrm{SFR}_{\mathrm{H}\alpha,\mathrm{uncorrected}}) = 0.55\log_{10}(\mathrm{SFR}_{1.4\,\mathrm{GHz}}) - 0.22. \quad (5)$$

The standard errors on the slope and intercept are both ±0.02, as estimated from the diagonal of the covariance matrix.

This is used to correct the local Universe, $0.0 < z < 0.35$, $0.01\,M_\odot\,\mathrm{dex}^{-1} < M < 11.6\,M_\odot\,\mathrm{dex}^{-1}$, and the fit becomes a close match to the data, following the approach of Hopkins et al. (2001). To evaluate the applicability of this method across evolving redshift, three additional SFR relationship models are developed. The first, Model 1 (shown as dashed line in Figure 2), assumes no correction, treating the SFRs derived from Hα and 1.4 GHz radio as equivalent. The other two models have slopes that lie between the 1:1 case and our fitted dust-correction model. These models are summarised in Table 1 where the fitted relationship shown in Equation (5) is now referred to as Model 4.

We also present two intermediate relations between the dust-free relation and the locally derived SFR relation.

These are based on an iterative procedure designed to determine the corrections required to reproduce star formation rate densities consistent with observations across different epochs of cosmic history.

It is useful to reconsider this plot after a full readthrough!

$$\log(\mathrm{SFR}_{1.4\,\mathrm{GHz}})$$
$$0.85\log(\mathrm{SFR}_{1.4\,\mathrm{GHz}}) - 0.07$$
$$_{\mathrm{H}\alpha,\mathrm{uncorrected}}) = 0.7\log(\mathrm{SFR}_{1.4\,\mathrm{GHz}}) - 0.14$$
$$_{\mathrm{H}\alpha,\mathrm{uncorrected}}) = 0.55\log(\mathrm{SFR}_{1.4\,\mathrm{GHz}}) - 0.22$$

Table 2. Correction factors converting uncorrected Hα star formation rates to radio-derived star formation rates as a function of redshift and uncorrected Hα luminosity. Correction factors are defined as the ratio $\mathrm{SFR}_{1.4\,\mathrm{GHz}}/\mathrm{SFR}_{\mathrm{H}\alpha,\mathrm{uncorrected}}$ and are shown for four representative uncorrected Hα luminosities. Luminosities are given in units of 10^{36} WHz^{-1}.

Redshift	Uncorrected Hα Luminosity (10^{36} W Hz^{-1})			
	0.25	0.8	2.5	8.0
0–0.5	1.0	2.5	6.5	16.7
0.5–1.5	1.0	1.5	2.6	4.3
1.5–3.0	1.0	1.2	1.5	1.8

The physical interpretation of these models relates to the inherent level of dust attenuation. The 1:1 case (Model 1) serves as a proxy for a dust-free Universe, in contrast, the fitted relationship (Model 4) reflects the current local Universe. Models 2 and 3, which fall between Models 1 and 4, therefore represent scenarios of intermediate dust attenuation. Our correction method works by inferring the level of dust attenuation from the observed radio SFR.

To apply this relationship for dust correction, we first convert the Hα luminosities to uncorrected star formation rates using the calibration from Kennicutt (1998), adjusted with the Chabrier IMF correction from Madau & Dickinson (2014). We then determine the corresponding dust-corrected SFR by finding its corresponding radio SFR, dust corrected based on the model applied. The corrected SFR is then subsequently converted back into a luminosity by reversing the same SFR calibration. The resulting luminosities are then compared to observations, as detailed in Section 4.

Calculating the correction factor for each luminosity and redshift-dependent calibration from uncorrected Hα SFRs to their radio-derived SFRs can be expressed as a multiplicative correction factor (CF). This factor is defined, for each of the three redshift ranges over which our models are applicable, as the ratio of the radio SFR to the uncorrected Hα SFR. Correction factors are computed for four representative uncorrected Hα luminosities and are presented in Table 2. This quantity effectively parameterises the deviation of each calibration from the one-to-one relation between Hα and radio SFRs (the resulting correction factors are tabulated in Table 2). These indicate that progressively smaller dust corrections are required at higher redshifts.

How does this relation affect us? - i.e. the Results

By taking an uncorrected SFR we can directly read off its corrected SFR!

Refitted Luminosity functions:

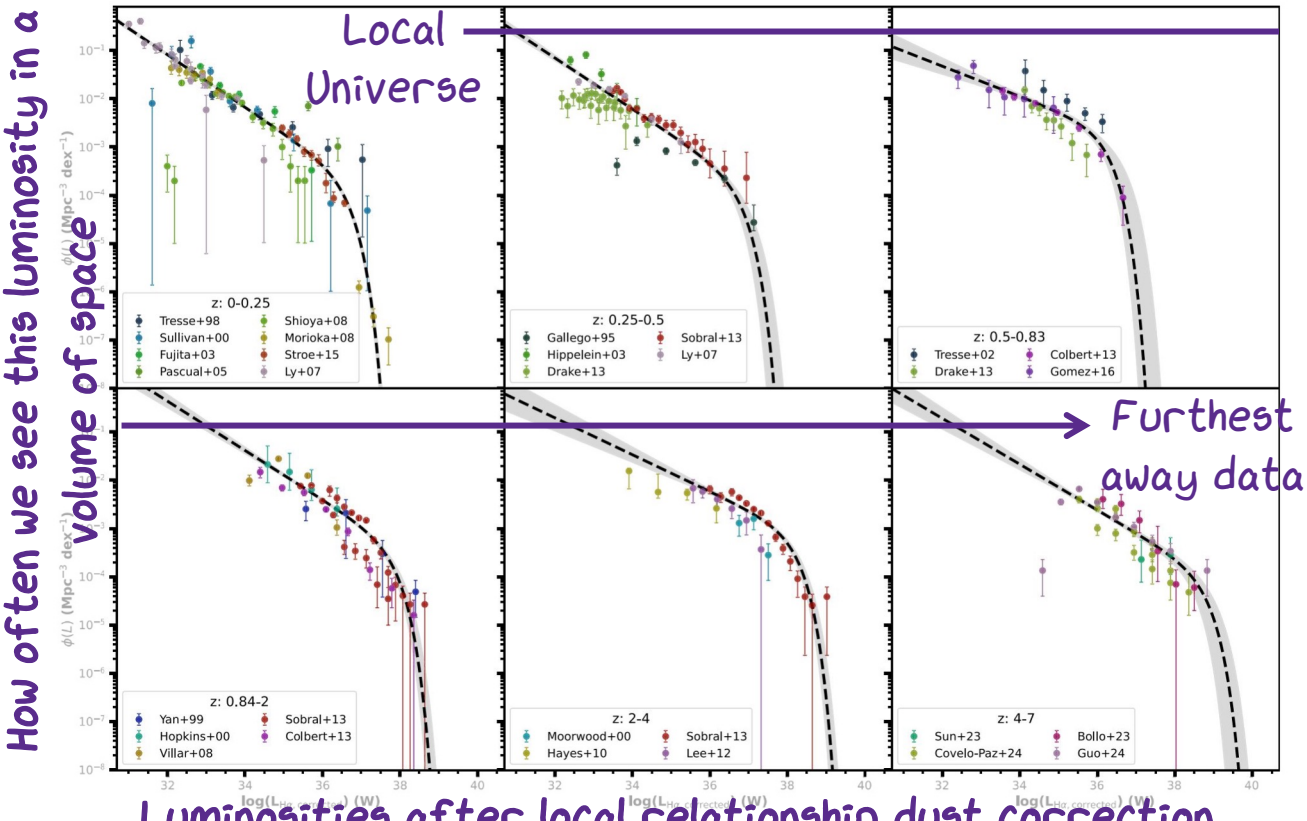

Figure 3. Published luminosity values, corrected for dust obscuration using the fitted SFR relation from Figure 2 (coloured symbols), along with the corresponding best-fit Schechter functions (dashed line), shown across six redshift bins. Where possible, raw luminosity data from these sources have been used; if necessary, published dust corrections were removed. Our fitted SFR-based dust correction relation (Model 4) was applied instead and new LFs were refitted, where the shaded region depicts the 95% confidence interval from 100 000 MCMC iterations. See Section 2.4 for relevant published Hα luminosity data.

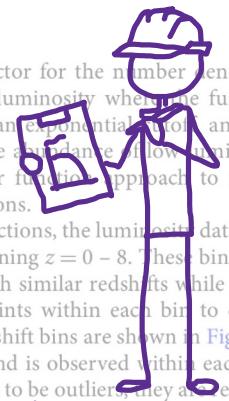

fit new LFs to the data. Allowing us to compare our approach with existing results and to evaluate how the relationship may vary with redshift by integrating to obtain the SFRD. Using the dust correction from the fitted relationship (Model 4) we present updated LFs in Figure 3. The luminosity values when using the radio-optical SFR based relationship as a dust correction are substantially brighter than in the original LFs, sitting up to two orders of magnitudes higher at all redshifts, compared to the original data.

How did we fit the new data?

1. Take all the Hα luminosity functions we can find
2. Turn them into SFRs
3. Apply our correction using the local relationship
4. Turn back into luminosity functions to refit and do analysis
5. Repeat to explore the other relationships (dust free, hypothesized other redshift models)

4.2. Fitting new luminosity functions

The LF, $\Phi(L)$, describes the number of galaxies per unit volume per luminosity interval. Named after astronomer Paul Schechter in observational cosmology that characterises the distribution of galaxy luminosities within the Universe. As galaxy luminosity is correlated with star formation activity, the LF is often used to study how star formation varies with galaxy population and redshift.

A widely used analytical form for modelling galaxy LFs in the optical regime is the Schechter function introduced by Schechter (1976) and given by:

$$\phi(L)\,dL = \phi^*\left(\frac{L}{L_*}\right)^{\alpha}\exp\left(-\frac{L}{L_*}\right)\frac{dL}{L_*} \quad (6)$$

where ϕ^* is the normalisation factor for the number density of galaxies, L_* is the characteristic luminosity where the function transitions from a power-law to an exponential form and α is the faint-end slope, describing the abundance of low luminosity galaxies. We adopt the Schechter function approach to fit the newly corrected luminosity functions.

To fit Schechter luminosity functions, the luminosity data were divided into six redshift bins spanning $z = 0 - 8$. These bins were chosen to group together data with similar redshifts while maintaining a sufficient density of points within each bin to enable statistically robust fitting. The redshift bins are shown in Figure 3, where a reasonably consistent trend is observed within each bin. Although some data points appear to be outliers, they are retained during fitting process. While the luminosity function refitting process accounts for reported uncertainties, other factors–such as survey area–can influence the results. Larger survey volumes increase the likelihood of detecting rarer, high-luminosity sources, which in turn affects the fitted values of parameters. This becomes especially significant at redshifts where observational scatter is high.

The redshift fitting was initially done with a chi-squared method by minimising the residuals, weighted by the uncertainties of the data points. To quantify the uncertainties in the fitted parameters, the initial solution was refined using a Markov Chain Monte Carlo (MCMC) approach implemented with the

https://doi.org/10.1017/pasa.2026.10183

Table 3. Best-fit parameters of Hα Luminosity function for maximum dust correction model, including reduced chi-squared (χ^2) values for each redshift bin.

This is the summary of all the new luminosity function fits with the four different corrections

Redshift	$\log(\phi^*)$	L^*	α	χ^2
0.0–0.25	-3.92 ± 0.03	36.54 ± 0.02	-1.54 ± 0.01	1.44
0.25–0.5	-3.49 ± 0.04	36.39 ± 0.03	-1.46 ± 0.02	0.79
0.5–0.83	-2.99 ± 0.10	36.17 ± 0.13	-1.31 ± 0.04	0.36
0.83–1.3	-3.16 ± 0.08	37.00 ± 0.07	-1.51 ± 0.02	1.00
2.0–4.0	-3.41 ± 0.06	38.14 ± 0.06	-1.38 ± 0.03	0.74
4.0–7.0	-4.27 ± 0.12	38.72 ± 0.17	-1.47 ± 0.03	0.92

Python package `emcee`, which uses MCMC to efficiently explore parameter space and estimate uncertainties for complex models (Foreman-Mackey et al. 2012).[c] The MCMC was run for 100 000 iterations for each redshift bin. The fitting procedure was repeated independently for the luminosity data corresponding to each of the four models. The best-fit luminosity function parameters for the local SFG SFR dust correction relation (Model 4) are reported in Table 3.

Calculating the overall effect

We can derive the cosmic SFRD, $\rho_{\rm SFR}$, via integration of the luminosity function to compute the luminosity density, ρ_L:

$$\rho_{\rm L} = \int_{L_{\rm lim}}^{\infty} L\Phi(L)dL = \phi^* L^* \Gamma(\alpha + 2, L_{\rm lim}/L^*), \quad (7)$$

This is the math we use to go from luminosity function to star formation rate density.

This is the lower luminosity limit of the integration which is often set by survey [illegible] a value of $L_{\rm lim} = 10^{30}$ W to account for the full range of the data. Through [illegible] minimal change in final SFRD value, with up to ≈2% difference when using values up to $L_{\rm lim} = 10^{36.6}$ W and no additional value when integrating to $L_{\rm lim} = 10^{0}$ W.

The luminosity density can then be converted into an estimate of the SFRD using a wavelength-dependent SFR calibration factor. These calibrations depend on the IMF and the choice of SFR tracer. For the Hα luminosity, we adopt the Kennicutt (1998) calibration, converted to an assumption of a Chabrier IMF:

$$\rho_{\rm SFR} = [illegible] \quad (8)$$

Here we outline the effects of each model as seen in the figure on the next page.

The cosmic SFRD provides a valuable means of tracing the evolution of SFR over cosmic time. The SFRD evolution for each of our four models is presented in Figure 4. This figure compares our results against single or compiled dust-corrected SFRDs from 33 [illegible] hs, see [illegible] s from [illegible].

[illegible] ship between SFR [illegible] tional data at low [illegible] [illegible] by the fitted relation exhibits an [illegible] early not well supported by existing measurements.

[c]https://emcee.readthedocs.io/.

If we apply the local dust correction relationship, then it works well for local observations but HUGELY overpredicts at high redshift.

[illegible] essively [illegible] timates [illegible] tion is [illegible] s with redshift [illegible] es. [illegible] uration [illegible] hs over [illegible] [illegible] method can serve as a promising alternative for estimating SFRs in the local Universe, particularly in cases where traditional obscuration corrections based on spectral line diagnostics or galaxy [illegible] methods are unavailable. Such [illegible] are common in large photometric or radio surveys where emission line data may be incomplete or of low quality (Prathap et al. 2025).

This is where those other two relationships come in!

Beyond $z \sim 1$, the SFR-dependent obscuration correction increasingly overestimates the SFRD, (Figure 4), with deviations reaching up to two orders of magnitude compared to published [illegible] s [illegible] p [illegible] values. In contrast, a steeper slope, such as that used in Model 3 (shown in dark orange in Figure 4), produces a markedly better [illegible] [illegible] smic noon', [illegible] d that the SFR-dependent obscuration correction requires a slope intermediate between that of Model 2 and Model 3 (shown in light and dark orange, respectively, in Figure 4) in order to approximate published values for the SFRD. Implying a transitional phase in the relationship between Hα and radio luminosities, possibly reflecting a balance between increasing dust production in rapidly evolving galaxies and the onset of more massive, dust-rich systems.

The steeper relationship or more dust free actually fits pretty nicely at high redshift.

The relationship closer to our local relationship fits best at intermediate redshifts.

The redshift range above $z \approx 3.0$, is marked by considerable scatter among different SFR tracers, reflecting a lack of consensus across methodologies (Bouwens et al. 2012; Schreiber et al. 2013; Novak et al. 2017; Bollo et al. 2023; Covelo-Paz et al. 2024). The variation [illegible] [illegible] [illegible] evolving ISM geometries, dust build up timescales and selection biases inherent in current high redshift galaxy samples. Recent JWST results also suggest that the emergence of a distinct population of red star-forming galaxies (RedSFGs) at $3 \lesssim z \lesssim 4$ may play a role in shaping this behaviour. Farrah et al. (2023) identify these RedSFGs as a possible evolutionary link between star-forming and quiescent galaxies, potentially contributing to the observed slope transition in this redshift range. It is worth noting that the Madau & Dickinson (2014) SFRD for $z > 3$ aligns almost identically with our Model 1, implying no dust obscuration at all. This is not likely to be physical, given the results noted above, and many others that measure non-negligible obscuration at high redshift.

In addition to observational factors, the evolution of galaxy metallicities with redshift may also play a role (Panter, Heavens,

The highlighted colors correspond to the lines on the next page!

Resulting amount of star formation if corrections are used:

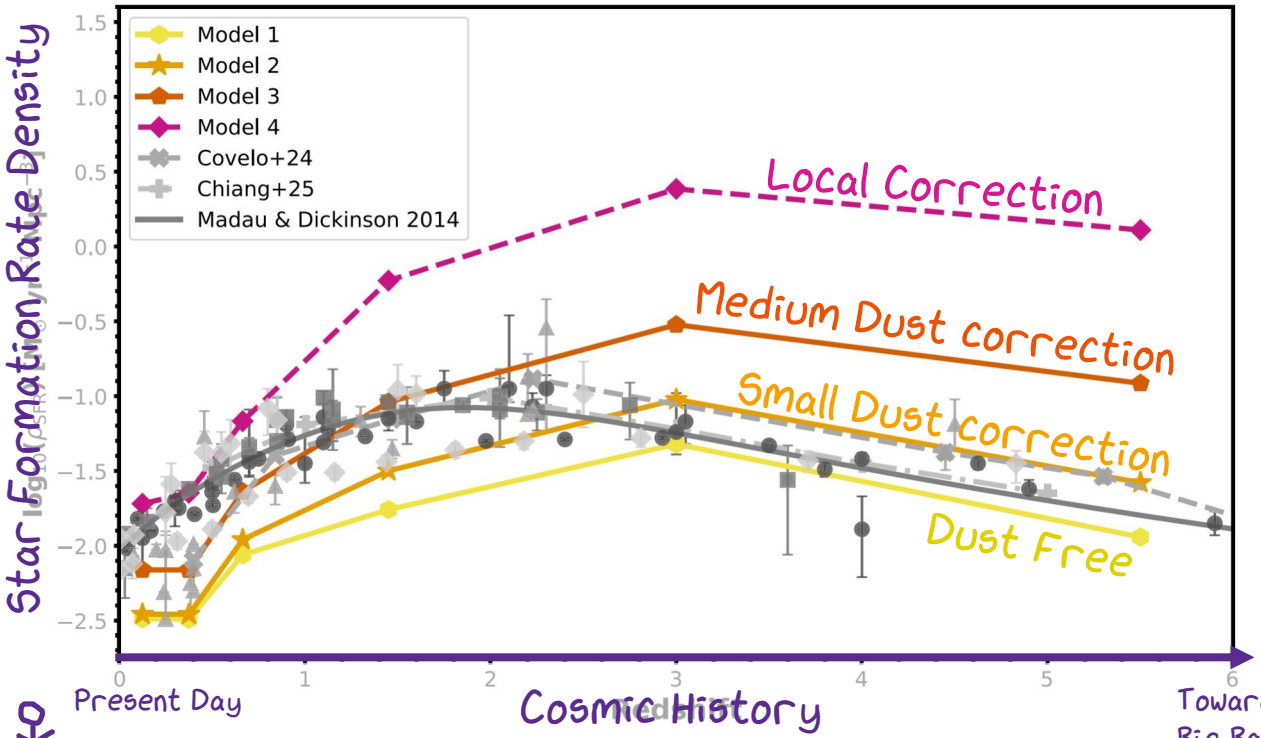

Figure 4. Cosmic SFRDs derived from dust-corrected luminosity functions using each of our four dust correction models, shown in Table 1. These results are compared with recent dust-corrected measurements from Covelo-Paz et al. (2024) and Chiang et al. (2025) in dashed and dot-dashed lines, respectively. The Madau & Dickinson (2014) relation is shown in solid grey for comparison. Published dust-corrected star formation rate density (SFRD) values are shown in grey, with markers indicating the observation (circles), Hα (triangles), infrared (squares), and radio (diamonds). The published data is compiled in Table A1.

If there is a different level of correction needed as we go back in cosmic history, then maybe we should make a correction that is both luminosity AND redshift dependent.

& Jimenez 2003; Camps-Fariña et al. 2022). Lower-metallicity galaxies, which are more common at higher redshifts, produce lower SFR for a given UV luminosity. Ignoring this by applying SFR–luminosity calibrations derived for predominantly solar-metallicity galaxies can lead to a significant systematic bias. While this effect is expected to be smaller than the observed discrepancy, it may still contribute to it; however, quantifying its impact lies beyond the scope of this work.

The fact that neither the steeper nor shallower correction alone accurately reproduces the observed star formation density implies that a single, static obscuration correction is inadequate across this redshift range. Instead, the obscuration characteristics may be evolving more dynamically. This is potentially influenced by variations in star formation modes (e.g. Kennicutt, Tamblyn, & Congdon, 1994; Yoachim, & Bernstein 2004; Holwerda et al. 2012; Holwerda et al. 2015) and is consistent with studies that highlights the need for either a smoothly evolving SFR–based dust calibration or a multi-parametric approach that accounts for additional galaxy properties beyond redshift alone.

Our dust correction model =

5. Recommended Model

These results indicate that the SFR-based dust correction must evolve with redshift to match optical based approaches, no single fit is appropriate. A composite model, constructed by combining the most consistent model across different redshift ranges, is proposed to describe the SFRD evolution. The models are used in with spline fit and then smoothed to create a sample model which is shown in Figure 5.

Here we adopt Model 4 in the redshift range $0 < z < 0.5$, based on the Hα and Radio SFR relationship in our local Universe which uses observational data in this redshift region. Then a smooth transition to Model 3 is applied for $0.5 < z < 1.5$. Then Model 2 out to redshift $z \approx 3$. In this redshift range, the Model should sit somewhere between Model 1 and 2. The redshift ranges over which each model best aligns with the observed cosmic SFRD are annotated in Figure 2. The composite model is expressed as a redshift- and luminosity-dependent correction factor in Equation (3), where K is the SFR calibration constant from Kennicutt (1998).

We therefore perform a spline fit between the models in the regimes where each provides the best agreement, producing a proposed dust-correction model.

$$\log\left(\frac{L_{H\alpha}}{K}\right)^{-2.22} \quad 0 \le z < 0.5,$$
$$\log\left(\frac{L_{H\alpha}}{K}\right)^{-3.33} \quad 0.5 \le z < 1, \qquad (9)$$
$$\log\left(\frac{L_{H\alpha}}{K}\right)^{-4.65} \quad 1 \le z < 3.$$

In practice, our prescription for applying a luminosity- and redshift-dependent dust obscuration correction is as follows: first, correct the observed Hα luminosity using Equation (3); next, convert this corrected luminosity into an uncorrected Hα SFR via

Our combined Luminosity and Redshift dependent dust correction model !!!

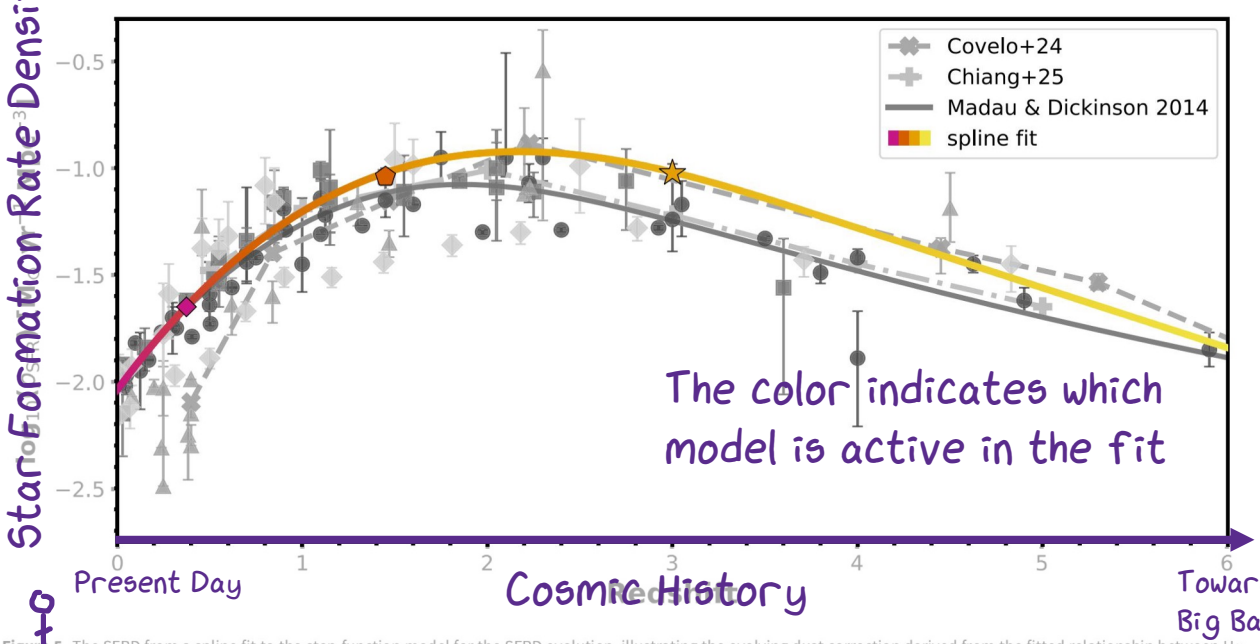

Figure 5. The SFRD from a spline fit to the step-function model for the SFRD evolution, illustrating the evolving dust correction derived from the fitted relationship between Hα and radio SFR tracers. Here the symbols are the same as in Figure 4. The colours of the spline fit correspond to those in Figure 4 for the model proposed in each redshift range from the 'local Universe dust content' scenario of Model 4 to the 'dust-free' scenario of Model 1. The data points where the spline fit changes model are shown by the markers, where the marker type represents the model as shown in Figure 4.

This may provide important insight into the evolution of dust content throughout the Universe, or at the very least into how dust attenuation is measured.

Our results suggest that the early Universe contained significantly less dust than is observed locally. Alternatively, this may indicate that dust in the early Universe is distributed or traced differently from what is currently assumed in existing models.

The Takeaways

We made a cool new way to correct optical light for dust beyond our local universe when we don't have all the traditional data methods to do this.

We use radio data to construct a correlation, that we can use to correct!

The local correction doesn't work throughout all cosmic history, so we try some other correction strengths.

This allows us to make an inferred redshift and luminosity dependent correction for dust! Woo!

We would like to thank... :-)

Thankyou to some people for minor comments on this work and also the telescope facilities for this cool data to play with!

I'm still working on turning this methodology into a self consistent python package - stay tuned!

This work uses a lot of contested ideas about dust, measurements, corrections, star formation etc. etc. that means we needed to cite a lot of people's ideas to convince you this works.

References:

Ahmed, U. T., et al. 2024, PASA, 41, e021
Arango-Toro, R. C., et al. 2023, A&A, 675, A126
Bail, A. L., et al. 2024, A&A, 688, A53
Baldwin, J. A., Phillips, M. M., & Terlevich, R. 1981, PASP, 93, 5
Bell, E. F. 2003, ApJ, 586, 794
Bellstedt, S., et al. 2020, MNRAS, 496, 3235
Bollo, V., et al. 2023, ApJ, 946, 117
Bouwens, R. J., et al. 2012, ApJ, 752, L5
Bouwens, R. J., et al. 2015, ApJ, 803, 34
Brown, M. J. I., et al. 2017, ApJ, 847, 136
Calzetti, D., et al. 2000, ApJ, 533, 682
Calzetti, D. 2001, PASP, 113, 1449
Calzetti, D., et al. 2007, ApJ, 666, 870
Camps-Fariña, A., et al. 2022, ApJ, 933, 44
Casey, C. M., et al. 2014, ApJ, 796, 95
Chabrier, G. 2003, PASP, 115, 763
Chiang, Y.-K., Makiya, R., & Ménard, B. 2025, ApJ, 992, 65
Planck Collaboration, et al. 2016, A&A, 594, A13
Condon, J. J. 1992, ARA&A, 30, 575
Condon, J. J., et al. 2002, AJ, 124, 675
Cook, R. H. W., et al. 2024, MNRAS, 531, 708
Covelo-Paz, A., et al. 2024, A&A, 694, A178
Cowley, M. J., et al. 2016, MNRAS, 457, 629
Dahlen, T., et al. 2007, ApJ, 654, 172
Dalcanton, J. J., Yoachim, P., & Bernstein, R. A. 2004, ApJ, 608, 189
Davies, L. J. M., et al. 2016, MNRAS, 461, 458
Davies, L. J. M., et al. 2017, MNRAS, 466, 2312
Delhaize, J., et al. 2017, A&A, 602, A4
Drake, A. B., et al. 2013, MNRAS, 433, 796
Driver, S. P., et al. 2009, A&G, 50, 5.12
Driver, S. P., et al. 2011, MNRAS, 413, 971
Driver, S. P., et al. 2018, MNRAS, 475, 2891
Driver, S. P., et al. 2022, MNRAS, 513, 439
Duncan, K. J., et al. 2020, MNRAS, 498, 3648
Edge, A., et al. 2013, Msngr, 154, 32
Enia, A., et al. 2022, ApJ, 927, 204
Farley, B., et al. 2025, PASA, 42, e067
Farrah, D., et al. 2008, ApJ, 677, 957
Finkelstein, S. L., et al. 2011, ApJ, 729, 140
Foreman-Mackey, D., Hogg, D. W., Lang, D., & Goodman, J. 2012, PASP, 125, 306
Fujita, S. S., et al. 2003, ApJ, 586, L115
Gallego, J., Zamorano, J., Aragon-Salamanca, A., & Rego, M. 1995, ApJ, 455, L1
Glazebrook, K., et al. 2004, AJ, 128, 2652
Glazebrook, K., Blake, C., Economou, F., Lilly, S., & Colless, M. 1999, MNRAS, 306, 843
Gómez-Guijarro, C., et al. 2022, ApJ, 956, 54
Gordon, Y. A., et al. 2017, MNRAS, 465, 2671
Gruppioni, C., et al. 2013, MNRAS, 432, 23
Gunawardhana, M. L. P., et al. 2011, MNRAS, 415, 1647
Gunawardhana, M. L. P., et al. 2013, MNRAS, 433, 2764
Guo, J., et al. 2013, ApJ, 767, 2
Gürkan, G., et al. 2022, MNRAS, 512, 6104
Haarsma, D. B., et al. 2000, ApJ, 544, 641
Hao, C.-N., et al. 2011, ApJ, 741, 124
Hayes, M., Schaerer, D., Östlin, G. 2010, A&A, 530, A15
Hippelein, H., et al. 2003, A&A, 402, 65
Holwerda, B. W., et al. 2012, ApJ, 753, 25
Holwerda, B. W., et al. 2013, ApJ, 766, 94
Hopkins, A. M., et al. 2003, ApJ, 599, 971
Hopkins, A. M., et al. 2009, arXiv:0910.4109
Hopkins, A. M., et al. 2025, PASA, arXiv:2505.08271 [astro-ph]
Hopkins, A. M., Connolly, A. J., Haarsma, D. B., & Cram, L. E. 2001, AJ, 122, 288
Hopkins, A. M., Connolly, A. J., & Szalay, A. S. 2000, AJ, 120, 2843
Ibar, E., et al. 2013, MNRAS, 434, 3218
Ivison, R. J., et al. 2010, A&A, 518, L31
Johnston, S., et al. 2007, PASA, 24, 174
Jong, J. T. A. d., et al. 2015, A&A, 582, A62
Kauffmann, G., et al. 2003a, MNRAS, 346, 1055
Kennicutt, Jr., R. C., 1998, ARA&A, 36, 189
Kennicutt, Jr., R. C. et al. 2009, ApJ, 703, 1672
Kennicutt, R. C., & Evans, N. J. 2012, ARA&A, 50, 531
Kewley, L. J., Dopita, M. A., Sutherland, R. S., Heisler, C. A., & Trevena, J. 2001, ApJ, 556, 121
Kreckel, K., et al. 2013, ApJ, 771, 62

Like a lot of people's ideas...

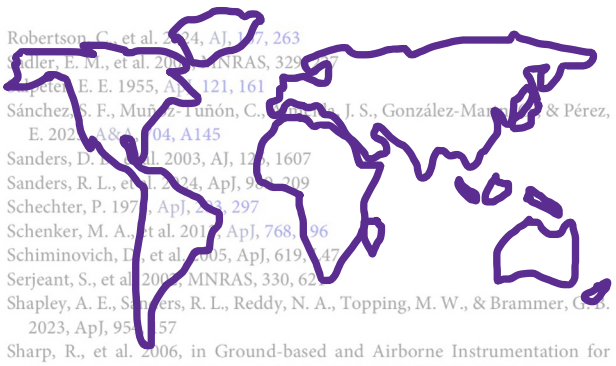

If you want to know more about certain parts of the method, you will probably find more details here.

Le Floc'h, E., et al. 2005, ApJ, 632, 169
Leauthaud, A., et al. 2012, MNRAS, 427, 1290
Lee, J. C., et al. 2009, ApJ, 706, 599
Liske, J., et al. 2015, MNRAS, 452, 2087
Ly, C., et al. 2007, ApJ, 657, 738
Machalski, J., et al. 2000, A&A, 360, 463
Madau, P., & Dickinson, M. 2014, ARA&A, 52, 415
Madau, P., & Fragos, T. 2017, ApJ, 840, 39
Magnelli, B., et al. 2011, A&A, 528, A35
Magnelli, B., et al. 2013, A&A, 553, A132
Matharu, J., et al. 2023, ApJL, 949, L11
Matthews, A. M., Condon, J. J., Cotton, W. D., & Mauch, T. 2021, ApJ, 914, 126
McConnell, D., et al. 2020, PASA, 37, e048
Molnár, D. C., et al. 2021, MNRAS, 504, 118
Moorwood, A. F. M., van der Werf, P. P., Cuby, J. G., & Oliva, E. 2000, A&A, 362, 9
Morioka, T., et al. 2008, PASJ, 60, 1219
Murphy, E. J., et al. 2011, ApJ, 737, 67
Norris, R. P., et al. 2011, PASA, 28, 215
Norris, R. P., et al. 2021, PASA, 38, e046
Novak, M., et al. 2017, A&A, 602, A5
Osterbrock, D. E. 1989, Astrophysics of Gaseous Nebulae and Active Galactic Nuclei. University Science Books in Mill Valley, California.
Panter, B., Heavens, A. F., & Jimenez, R. 2003, MNRAS, 343, 1145
Pascual, S., et al. 2005, in Revista Mexicana de Astronomia y Astrofisica Conference Series, Vol. 24, Revista Mexicana de Astronomia y Astrofisica Conference Series, ed. A. M. Hidalgo-Gámez, J. J. González, J. M. Rodrguez Espinosa, & S. Torres-Peimbert, 268
Pérez-González, P. G., et al. 2005, ApJ, 630, 82
Pontoppidan, K., et al. 2022, ApJL, 936, L14
Pope, A., et al. 2008, ApJ, 675, 1171
Prathap, J., et al. 2024, PASA, 41, e016
Prathap, J., et al. 2025, PASA, 42, e077
Reddy, N. A., et al. 2009, ApJ, 692, 778
Reddy, N. A., Topping, M. W., Sanders, R. L., Shapley, A. E., & Brammer, G. 2023, ApJ, 948, 83
Rinaldi, P., et al. 2023, ApJ, 952, 143
Robertson, C., et al. 2024, AJ, 167, 263
Sadler, E. M., et al. 2007, MNRAS, 329, 227
Peterson, E. E. 1955, ApJ, 121, 161
Sánchez, S. F., Muñoz-Tuñón, C., Mollá, J. S., González-Martín, O. & Pérez, E. 2024, A&A, 684, A145
Sanders, D. B., et al. 2003, AJ, 126, 1607
Sanders, R. L., et al. 2024, ApJ, 966, 209
Schechter, P. 1976, ApJ, 203, 297
Schenker, M. A., et al. 2013, ApJ, 768, 196
Schiminovich, D., et al. 2005, ApJ, 619, 47
Serjeant, S., et al. 2003, MNRAS, 330, 621
Shapley, A. E., Sanders, R. L., Reddy, N. A., Topping, M. W., & Brammer, G. B. 2023, ApJ, 954, 157
Sharp, R., et al. 2006, in Ground-based and Airborne Instrumentation for Astronomy, ed. I. S. McLean, & M. Iye, Vol. 6269 (SPIE), 62690G
Shioya, Y., et al. 2008, ApJS, 175, 128
Smith, G. A., et al. 2004, in Society of Photo-Optical Instrumentation Engineers (SPIE) Conference Series, Vol. 5492, Ground-based Instrumentation for Astronomy, ed. A. F. M. Moorwood, & M. Iye, 410
Sobral, D., et al. 2013, MNRAS, 428, 1128
Stach, S. M., et al. 2018, ApJ, 860, 151
Strolger, A.-L., Riess, A. G., Dahlen, T., et al. 2010, AJ, 139, 962
Sullivan, M., et al. 2000, MNRAS, 312, 442
Sun, F., et al. 2023, ApJ, 953, 53
Takeuchi, T. T., et al. 2003, ApJ, 587, L89
Tarrasse, M., et al. 2025, A&A, 697, A181
Taylor, E. N., et al. 2011, MNRAS, 418, 1587
Terao, Y., et al. 2022, ApJ, 941, 70
Thomson, A., et al. 2017, ApJ, 838, 119
Tresse, L., & Maddox, S. J. 1998, ApJ, 495, 691
Veilleux, S., & Osterbrock, D. E. 1987, ApJS, 63, 295
Villar, V., et al. 2008, ApJ, 677, 169
Wright, E. L., et al. 2010, AJ, 140, 1868
Wyder, T. K., et al. 2005, ApJ, 619, L15
Yan, L., et al. 1999, ApJ, 519, L47
Yuan, T.-T., Kewley, L. J., & Rich, J. 2013, ApJ, 767, 106
Yun, M. S., Reddy, N. A., & Condon, J. J. 2001, ApJ, 554, 803

Appendix A.

Here is a table that shows all the star formation rate densities that took months to find, put into the same units, and correct so they had the same underlying physics...

Table A1. Measurements of the star formation rate density, ρ_{SFR}, as a function of redshift.

Reference	Estimator	Redshift	$\log(\rho_{SFR})^a$	Reference	Estimator	Redshift	$\log(\rho_{SFR})^a$
Wyder et al. (2005)	UV	0.01–0.1	$-2.02^{}_{-0.02}$	Terao et al. (2022)	Hα	2.1–2.5	$-0.54^{+0.19}_{-0.70}$
Schiminovich et al. (2005)	UV	0.2–0.4	$-1.57^{+0.05}_{-0.06}$	Sobral & Matthee (2019)	Hα	0.08–0.25	$-2.03^{+0.04}_{0.00}$
		0.4–0.6	$-1.59^{+0.15}_{-0.08}$		Hα	0.5–0.8	$-1.64^{+0.12}_{-0.14}$
		0.6–0.8	$-1.40^{+0.31}_{-0.13}$	Drake et al. (2013)	Hα	0.0–0.35	$-2.49^{+0.59}_{0.00}$
		0.8–1.2	$-1.45^{+0.31}_{-0.13}$			0.0–0.5	$-2.15^{+0.02}_{-0.02}$
		0.6–0.8	$-1.44^{+0.1}_{-0.1}$	Hayes et al. (2010)	Hα	2.18–2.21	$-0.87^{+0.15}_{-0.24}$
		0.8–1.0	$-1.19^{+0.09}_{-0.08}$	Ly et al. (2007)	Hα	0.07–0.09	$-2.07^{+0.00}_{0.00}$
		1.0–1.2	$-1.14^{+0.09}_{-0.09}$			0.23–0.25	$-2.31^{+0.00}_{0.00}$
		1.2–1.7	$-1.15^{+0.15}_{-0.08}$			0.39–0.41	$-1.99^{+0.00}_{0.00}$
		1.7–2.5	$-0.95^{+0.49}_{-0.09}$	Yan et al. (1999)	Hα	0.7–1.9	$-1.16^{+0.09}_{-0.11}$
		2.5–3.5	$-1.24^{+0.26}_{-0.15}$	Moorwood et al. (2000)	Hα	1.3–2.2	$-1.12^{+0.00}_{0.00}$
		3.5–4.5	$-1.89^{+0.22}_{-0.32}$	Hippelein et al. (2003)	Hα	0.238–0.252	$-2.03^{+0.10}_{-0.13}$
Dahlen et al. (2007)	UV	0.92–1.33	$-1.22^{+0.08}_{-0.08}$	Glazebrook et al. (2004)	Hα	0.378–0.39	$-2.25^{+0.14}_{-0.21}$
		1.62–1.88	$-0.95^{+0.12}_{-0.12}$			0.452–0.464	$-1.27^{+0.17}_{-0.14}$
		2.08–2.37	$-1.07^{+0.09}_{-0.09}$	Sanders et al. (2003)	IR	0.03	$-1.92^{+0.02}_{-0.03}$
Reddy et al. (2009)	UV	1.9–2.7	$-0.95^{+0.09}_{-0.11}$	Takeuchi et al. (2003)	IR	0.03	$-2.15^{+0.20}_{-0.20}$
		2.7–3.4	$-1.17^{+0.11}_{-0.15}$	Magnelli et al. (2011)	IR	0.40–0.70	$-1.54^{+0.22}_{-0.11}$

Table A1. (Continued).

Reference	Estimator	Redshift	$\log(\rho_{SFR})^a$	Reference	Estimator	Redshift	$\log(\rho_{SFR})^a$
Bouwens et al. (2012)	UV	3.8	$-1.49^{+0.05}_{-0.05}$			0.70–1.00	$-1.16^{+0.15}_{-0.19}$
		4.9	$-1.62^{+0.06}_{-0.06}$			1.00–1.30	$-1.09^{+0.27}_{-0.21}$
		5.9	$-1.85^{+0.08}_{-0.08}$			1.30–1.80	$-1.11^{+0.17}_{-0.21}$
		7.0	$-1.99^{+0.1}_{-0.1}$			1.80–2.30	$-1.09^{+0.21}_{-0.25}$
		7.9	$-2.29^{+0.11}_{-0.11}$	Magnelli et al. (2013)	IR	0.40–0.70	$-1.42^{+0.08}_{-0.11}$
Schenker et al. (2013)	UV	7.0	$-2.20^{+0.1}_{-0.11}$			0.70–1.00	$-1.30^{+0.10}_{-0.13}$
		8.0	$-2.41^{+0.14}_{-0.14}$			1.00–1.30	$-1.16^{+0.13}_{-0.20}$
Driver et al. (2018)	UV	0.06–0.14	$-1.82^{+0.01}_{-0.01}$			1.30–1.80	$-1.14^{+0.13}_{-0.18}$
		0.14–0.20	−1.90			1.80–2.30	$-1.00^{+0.18}_{-0.15}$
		0.20–0.28	−1.77	Gruppioni et al. (2013)	IR	0.00–0.30	$-1.84^{+0.09}_{-0.11}$
		0.28–0.36	−1.75			0.30–0.45	$-1.62^{+0.03}_{-0.04}$
		0.36–0.45	$-1.79^{+0.01}_{-0.01}$			0.45–0.60	$-1.52^{+0.05}_{-0.05}$
		0.45–0.56	$-1.73^{+0.01}_{-0.01}$			0.60–0.80	$-1.34^{+0.06}_{-0.06}$
		0.56–0.68	−1.56			0.80–1.00	$-1.14^{+0.05}_{-0.06}$
		0.68–0.82	$-1.42^{+0.01}_{-0.01}$			1.00–1.20	$-1.01^{+0.04}_{-0.05}$
		0.82–1.00	−1.29			1.20–1.70	$-1.04^{+0.04}_{-0.04}$
		1.00–1.20	−1.31			1.70–2.00	$-1.06^{+0.02}_{-0.03}$
		1.20–1.45	−1.27			2.00–2.50	$-1.11^{+0.09}_{-0.12}$
		1.45–1.75	−1.17			2.50–3.00	$-1.06^{+0.15}_{-0.23}$
		1.75–2.20	$-1.30^{+0.01}_{-0.01}$			3.00–4.20	$-1.56^{+0.23}_{-0.50}$
		2.20–2.60	$-1.29^{+0.01}_{-0.01}$	Novak et al. (2017)	Radio	0.102 – 0.4	$-1.97^{+0.047}_{-0.052}$
		2.60–3.25	$-1.28^{+0.01}_{-0.01}$			0.401–0.6	$-1.89^{+0.045}_{-0.050}$
		3.25–3.75	$-1.33^{+0.01}_{-0.01}$			0.6–0.805	$-1.67^{+0.044}_{-0.048}$
		3.75–4.25	$-1.42^{+0.04}_{-0.04}$			0.803–1.0	$-1.51^{+0.044}_{-0.048}$
		4.25–5.00	$-1.45^{+0.04}_{-0.04}$			1.0–1.3	$-1.51^{+0.043}_{-0.049}$
Covelo-Paz et al. (2024)	Hα	3.8–5.1	$-1.38^{+0.05}_{-0.12}$	Enia et al. (2022)	Radio	0.1–0.4	$-1.78^{+0.24}_{-0.24}$
		4.9–5.7	$-1.54^{+0.04}_{0.00}$			0.4–0.7	$-1.38^{+0.14}_{-0.14}$
		5.7–6.6	$-1.85^{+0.11}_{-0.54}$			0.7–1.0	$-1.16^{+0.16}_{-0.16}$
Bollo et al. (2023)	Hα	3.86–4.94	$-1.19^{+0.16}_{-0.16}$			1.0–2.0	$-0.96^{+0.17}_{-0.17}$
Rinaldi et al. (2023)	Hα	7–8	$-2.35^{+0.30}_{0.00}$			2.0–3.0	$-0.99^{+0.22}_{-0.22}$
Sobral et al. (2013)	Hα	0.35–0.45	$-2.30^{+0.10}_{0.00}$	Condon et al. (2002)	Radio	0.0–0.1	$-2.16^{+0.03}_{-0.03}$
		0.75–0.95	$-1.60^{+0.07}_{-0.12}$	Sadler et al. (2002)	Radio	0.0–0.16	$-1.93^{+0.08}_{-0.09}$
		1.35–1.55	$-1.35^{+0.06}_{-0.07}$	Serjeant et al. (2002)	Radio	0.0–0.02	$-1.95^{+0.08}_{-0.10}$
		1.7–2.8	$-1.09^{+0.03}_{-0.03}$	Machalski et al. (2000)	Radio	0.0–0.14	$-2.12^{+0.10}_{-0.10}$
				Haarsma et al. (2000)	Radio	0.010–0.401	$-1.59^{+0.14}_{-0.21}$
						0.410–0.518	$-1.38^{+0.14}_{-0.20}$
						0.548–0.698	$-1.32^{+0.16}_{-0.26}$
						0.724–0.884	$-1.08^{+0.13}_{-0.18}$
						0.960–4.420	$-0.99^{+0.12}_{-0.18}$

[a]Calibrated for Chabrier IMF where needed.

Oh and some more ...

Please someone use them ...

I beg ...

This annotated version was made by:
Jayde Willingham
Aka the first author!